Asymmetric oscillations of endoskeletal antibubbles

Nobuki Kudo[1]*, Rustem Uzbekov[2,3], Ryonosuke Matsumoto[1], Ri-ichiro Shimizu[1], Craig S. Carlson[4], Nicole Anderton[4], Aurélie Deroubaix[5], Clement Penny[5], Albert T. Poortinga[6], David M. Rubin[4], Ayache Bouakaz[7], and Michiel Postema[2]

[1]*Faculty of Information Science and Technology, Hokkaido University, 9 Chome Kita 14 Jonishi, Kita Ward, Sapporo, Hokkaido 060-0814, Japan*
[2]*Department of Microscopy, Faculty of Medicine, University of Tours, 10 Boulevard Tonnellé, 37000 Tours, France*
[3]*Faculty of Bioengineering and Bioinformatics, Moscow State University, ul. Leninskiye Gory 1/73, Moscow 119192, Russia*
[4]*School of Electrical and Information Engineering, University of the Witwatersrand, Johannesburg, 1 Jan Smuts Laan, 2050 Braamfontein, South Africa*
[5]*Department of Internal Medicine, University of the Witwatersrand, Johannesburg, 1 Jan Smuts Laan, 2050 Braamfontein, South Africa*
[6]*Department of Mechanical Engineering, Eindhoven University of Technology, De Zaale, 5600 MB Eindhoven, Netherlands*
[7]*Inserm U1253, Faculty of Medicine, University of Tours, 10 Boulevard Tonnellé, 37000 Tours, France*

Antibubbles, *i.e.*, gas bubbles containing an incompressible core, have been under investigation as potential vehicles in ultrasound-guided drug delivery. It is assumed that antibubbles can expand unhampered, but cannot contract beyond the size of their inner core. In this study, this so-called expansion-only hypothesis is tested on endoskeletal antibubbles and reference bubbles. Antibubbles and identical bubbles without a core were subjected to short 3-cycle pulses of 1-MHz ultrasound, whilst being recorded with a high-speed camera operating at 10 million frames per second. At low acoustic amplitudes (200 kPa), antibubbles and bubbles oscillated symmetrically. At high acoustic amplitudes (1.00 MPa), antibubbles and bubbles oscillated asymmetrically, but antibubbles significantly more so than bubbles. Furthermore, fragmentation and core release were observed at these amplitudes. The high-speed videos confirm the expansion-only hypothesis at 1-MPa acoustic amplitude at a transmitting frequency of 1 MHz. One short, high-amplitude pulse appeared to be enough to shatter antibubbles and release their core contents. This finding may have implications for ultrasound-guided drug delivery using antibubbles.

1. Introduction

Ultrasound contrast agents consist of suspensions with micrometer-sized gas bubbles, each surrounded by a stabilising shell.[1)] In ultrasound fields, these so-called microbubbles oscillate, *i.e.*, they subsequently expand and contract, creating a secondary sound field that can be detected with imaging equipment. Consequently, injections of ultrasound contrast agents have been utilised for diagnostic medical imaging.[2–4)] Oscillating microbubbles may interact with living cells and tissue.[5–7)] Therefore, ultrasound contrast agents have also, more recently, been introduced in therapeutic settings.[8–10)] One of the most popular ways to study microbubbles subjected to ultrasound is with high-speed photography.[11–14)] Antibubbles are gas bubbles in suspension containing a liquid core droplet. Antibubbles with surfactant interfaces are short-lived, with drainage times within 1000 seconds.[15,16)] By adding nanoparticles to the interfaces, antibubbles can be produced with long lifespans.[17,18)] Antibubbles have been produced with microfluidics, too.[19)] Please note that the droplets are hanging inside the bubbles owing to electrostatic forces. By adding a hydrophobic endoskeleton, the droplets can be fixed in position inside the bubble. Endoskeletal antibubbles have been recently demonstrated.[21)] Figure 1 shows a bright-field microscopic image of endoskeletal antibubbles. Four antibubbles contain a single droplet core of approximately 5-μm diameter. The endoskelotons themselves are shown in Figure 2. The silica particles on the outer interface have been reported to form a single elastic layer.[22)] Shortly after the first high-speed camera observation of ultrasonic antibubbles, they were proposed as a vehicle to carry drugs to a region of interest, which are to be released using clinical ultrasound.[20)] Antibubbles have proven to be suitable ultrasound contrast agents for harmonic

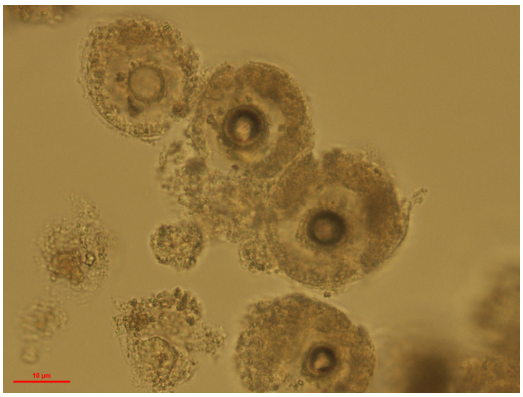

Fig. 1. Bright-field microscopic image of four endoskeletal antibubbles, with approximate inner droplet diameters of 5 μm. The scaling bar corresponds to 10 μm.

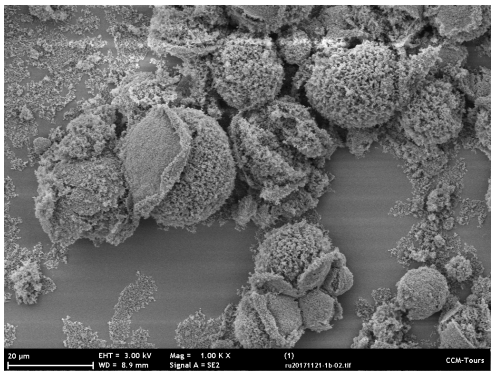

Fig. 2. Scanning electron microscope image of an endoskeletal antibubble. Ruptured silica membranes reveal skeletal structures underneath. The scaling bar corresponds to 10 μm. This image is a zoomed-out version of Fig. 1 in Ref. 21.

*E-mail: kudo@ist.hokudai.ac.jp

imaging, as well.[22] The unique harmonic features of antibubbles have been attributed to the assumption that antibubbles can expand unhampered, but cannot contract beyond the size of their inner core.[23] In a simulation study, the outward expansion has been shown to surpass that of bubbles without a core droplet, whilst the contraction of antibubbles is less than that of bubbles without core droplet.[24] Antibubbles have a higher resonance frequency than their bubble counterparts.[25] By modifying eq. (2.2.7) in Ref. 25 to contain the entire volumetric incompressible content V_i and ignoring the presence of an outer elastic shell, the linear resonance frequency f_r of the endoskeletal antibubble becomes:

$$f_\mathrm{r} = \frac{1}{2\pi R_0\sqrt{\rho}}\sqrt{\frac{3\gamma\left(p_0 - p_\mathrm{v} + \frac{2\sigma}{R_0}\right)}{1-\frac{3V_\mathrm{i}}{4\pi R_0^3}} - \frac{2\sigma}{R_0} - \frac{4\eta^2}{R_0^2\rho}}, \qquad (1)$$

where p_0 is the ambient pressure, p_v is the vapour pressure, R_0 is the equilibrium bubble radius, γ is the polytropic exponent of the gas, η is the liquid viscosity, ρ is the liquid density, and σ is the surface tension. Obviously, $0 \leq V_\mathrm{i} < \frac{4}{3}\pi R_0^3$. Thus, the presence of an endoskeleton increases the resonance frequency even more.

2. Methods

Two media containing (anti)bubbles were prepared for evaluation, as previously published.[18,22] For stabilisation, Aerosil® R972 hydrophobised silica particles (Evonik Industries AG, Essen, Germany) were used.[22] For the first medium, hereafter referred to as AB, the aqueous cores were replaced by 2 vol% of hydrophobically modified Zano 10 Plus zinc oxide nanoparticles (Umicore, Brussel, Belgium). The second medium was left without cores, so it contained stabilised bubbles instead of antibubbles. This medium served as reference medium, hereafter referred to as REF. For each medium, 5 mg of freeze-dried material was deposited into a FALCON® 15 mL High-Clarity Polypropylene Conical Tube (Corning Science México S.A. de C.V., Reynosa, Tamaulipas, Mexico), after which 5 mL of 049-16797 Distilled Water (FUJIFILM Wako Pure Chemical Corporation, Chuo-Ku, Osaka, Japan) was added. Each emulsion was gently shaken by hand for 1 minute, after which 200 μL was pipetted into the observation chamber of a high-speed observation system.[26] The observation chamber was placed under an IX70 microscope (Olympus Corporation, Shinjuku-ku, Tokyo, Japan) with a LUMPlan FI/IR 40× (N.A. 0.8) objective lens. Attached to the microscope was an HPV-X2 high-speed camera (Shimadzu, Nakagyo-ku, Kyoto, Japan), operating at 10 million frames per second.[27] During camera recording, the materials were subjected to ultrasound pulses, each comprising 3 cycles with a centre transmitting frequency of 1.00 MHz and a peak-negative pressure of 200 kPa (1 V input) or 1.00 MPa (5 V input), from a laboratory-assembled single-element transducer.[26,27] The transducer was driven by a signal generated by an AFG320 arbitrary function generator (Sony-Tektronix, Shinagawa-ku, Tokyo, Japan) and amplified by a UOD-WB-1000 wide-band power amplifier (TOKIN Corporation, Shiroishi, Miyagi, Japan). The videos recorded were segmented and analysed using MATLAB® (The MathWorks, Inc., Natick, MA, USA). In the first frame of each video, objects in the field of view were identified. These were then automatically sized throughout the rest of the video, resulting in radius(time) curves. For each radius(time) curve, the equilibrium radius, R_0, the maximum radius during the first cycle, R_max, and the first minimum radius after the transient phase, R_min, were determined. From these, the derivative values positive excursion, $\xi^+ = (R_\mathrm{max} - R_0)$, and negative excursion, $\xi^- = (-R_\mathrm{min} + R_0)$, were determined, yielding the absolute oscillation asymmetry $(\xi^+ - \xi^-) = (R_\mathrm{max} + R_\mathrm{min} - 2R_0)$.

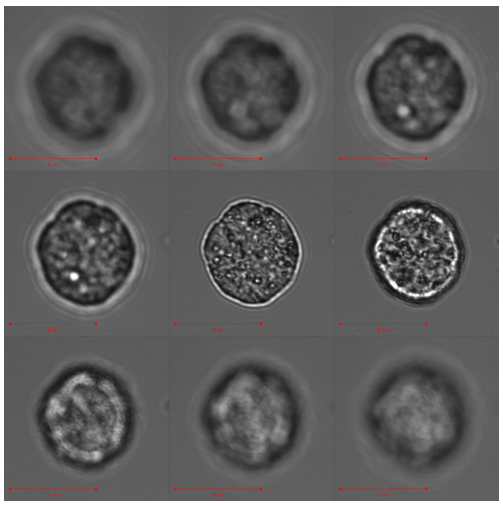

Fig. 3. Confocal microscopy z-stacks of AB. The scaling bars correspond to 10 μm.

3. Results

Figure 3 shows a z-stack of confocal microscopy images of an endoskeletal antibubble. In the focal plane (middle frame), droplets of diameters less than 1 μm can be observed, indicated by dark spots, an well as entrapped gas, indicated by white spots. Figure 4 shows the equilibrium radius R_0 versus the maximum expansion R_max and contraction R_min measured from a total of thirty-three high-speed videos with 118 AB and 144 REF, for acoustic pressure amplitudes of 200 kPa and 1.00 MPa, with their respective least-squares regression lines. At 200-kPa acoustic amplitude, REF has slightly higher excursions than AB. At 1.00-MPa amplitude, AB has substantially greater expansion ($R_\mathrm{max} = 1.5R_0 + 1.5$), wheres REF has greater contraction ($R_\mathrm{min} = 0.57R_0 + 0.07$). This is even more evident from the difference in least-squares solutions. At 200-kPa amplitude, for both AB and REF, $(\xi^+ - \xi^-) \approx 0$, *i.e.*, both oscillate symmetrically despite occasional asymmetry. However, at 1.00-MPa amplitude, for AB: $(\xi^+ - \xi^-) = 0.30R_0 + 1.2$, whereas for REF, $(\xi^+ - \xi^-) = 0.20R_0 + 1.5$. Thus, although both AB and REF oscillate asymmetrically, AB oscillates significantly more asymmetrically than REF.

Interestingly, in the same high-amplitude regime, the antibubbles can be observed to release their core contents. Fig. 5 shows 4 frames selected from 256 frames of a high-speed video with AB sonicated at a 1.00-MPa amplitude. After the first oscillation cycle, the surface instabilities leading to fragmentation can be clearly appreciated. After sonication, the antibubble fragments were scattered around the remains of a bubble. This bubble remained acoustically active during subsequent pulses (not shown). While low-amplitude pulses did not change the contents of the antibubble,[21] a short high-amplitude pulse could disrupt antibubbles within three cycles.

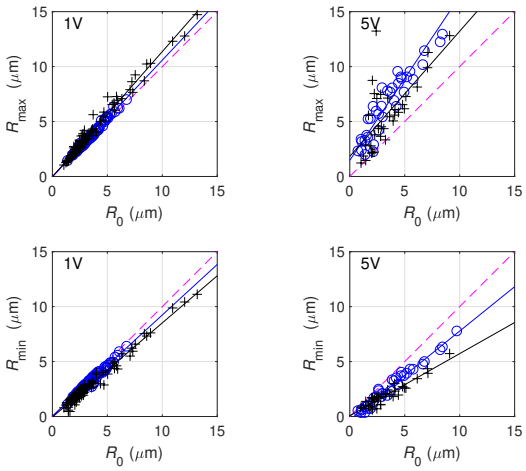

Fig. 4. Equilibrium radius R_0 versus maximum expansion R_{max} (top) and contraction R_{min} (bottom), for acoustic pressure amplitudes of 200 kPa (1V, left) and 1.00 MPa (5V, right). The dashed purple lines correspond to $R_{m*} = R_0$, the blue and black lines represent the least-squares solutions for AB (o) and REF (+), respectively.

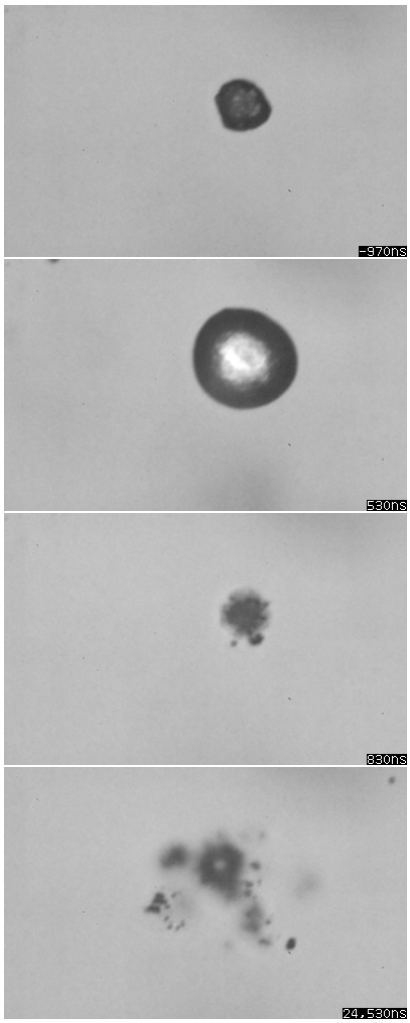

Fig. 5. Four high-speed frames of sonicated AB. Top-bottom: before sonication; during the first rarefactional peak; fragmentation during contraction; after sonication. Each frame width corresponds to 145 μm. Time stamps indicate −970 ns, 530 ns, 830 ns, and 24,530 ns.

4. Conclusions

The high-speed videos confirm the expansion-only hypothesis at 1-MPa acoustic amplitude at a transmitting frequency of 1 MHz. One short, high-amplitude pulse appeared to be enough to shatter antibubbles and release their core contents. This finding may have implications for ultrasound-guided drug delivery using antibubbles.

Acknowledgements The scanning electron microscope data were obtained with the aid of the IBiSA Electron Microscopy Facility of the University of Tours and the University Hospital of Tours.

1) V. Paefchen, D. Doleschel, and F. Kiessling, Front. Pharmacol. **6** 197 (2015).
2) S. Ishikura, M. Yoshizawa, N. Tagawa, and T. Irie, Jpn. J. Appl. Phys. **57** 07LF20 (2018).
3) R. R. Wildeboer, R. J. G. van Sloun, P. Huang, H. Wijkstra, and M. Mischi, Ultrasound Med. Biol. **45** 2713 (2019).
4) J. Quan, Y. Hong, X. Zhang, M. Mei, X. You, and P. Huang, Clin. Hemorheol. Microcirc. **72** 293 (2019).
5) R. Oitate, A. Shimomura, H. Wada, T. Mochizuki, K. Masuda, Y. Oda, R. Suzuki, and K. Maruyama, Jpn. J. Appl. Phys. **56** 07JF25 (2017).
6) R. Oitate, T. Otsuka, M. Seki, A. Furutani, T. Mochizuki, K. Masuda, R. Suzuki, and K. Murayama, Jpn. J. Appl. Phys. **57** 07LF10 (2018).
7) T. Sato and K. Ikeda, Jpn. J. Appl. Phys. **57** 07LF16 (2018).
8) S. Kotopoulis, G. Dimcevski, O. H. Gilja, D. Hoem, and M. Postema, Med. Phys. **40** 072902 (2013).
9) R. H. Rahayu, K. Takanashi, T. T. K. Soon, I. Seviaryna, R. Maev, K. Kobayashi, N. Hozumi, and S. Yoshida, Jpn. J. Appl. Phys. **56** 07LF26 (2017).
10) Wang G, Li Q, Chen D, Wu B, Wu Y, Tong W, and Huang P. Theranostics **9** 6191 (2019).
11) M. Postema, A. van Wamel, F. J. ten Cate, and N. de Jong, Med. Phys. **32** 3707 (2005).
12) K. Suzuki, R. Iwasaki, R. Takagi, S. Yoshizawa, and S. Umemura, Jpn. J. Appl. Phys. **56** 07JF27 (2017).
13) N. Okada, M. Shiiba, S. Yamauchi, T. Sato, and S. Takeuchi, Jpn. J. Appl. Phys. **57** 07LE15 (2018).
14) S. Nishitaka, D. Mashiko, S. Yoshizawa, and S. Umemura, Jpn. J. Appl. Phys. **57** 07LF25 (2018).
15) B. Scheid, S. Dorbolo, L. R. Arriaga, and E. Rio, Phys. Rev. Lett. **109** 264502 (2012).
16) Y. Vitry, S. Dorbolo, J. Vermant, and B. Scheid, Adv. Colloid Interface Sci. **270** 73 (2019).
17) A. T. Poortinga, Langmuir **27** 2138 (2011).
18) A. T. Poortinga, Colloid. Surf. A: Physicochem. Eng. Aspects **419** 15 (2013).
19) J. E. Silpe, J. K. Nunes, A. T. Poortinga, and H. A. Stone, Langmuir **29** 8782 (2013).
20) M. Postema, N. de Jong, G. Schmitz, and A. van Wamel, Proc. 2005 IEEE Ultrason. Symp. 977 (2005).
21) N. Kudo, R. Uzbekov, R. Matsumoto, R. Shimizu, C. Carlson, N. Anderton, A. Deroubaix, C. Penny, A. T. Poortinga, D. M. Rubin, A. Bouakaz, and M. Postema, Proc. 40th Symp. UltraSon. Electron. (2019).
22) M. Postema, A. Novell, C. Sennoga, A. T. Poortinga, and A. Bouakaz, Appl. Acoust. **137** 148 (2018).
23) K. Johansen and M. Postema, Hydroacoustics **19** 197 (2016).
24) K. Johansen, S. Kotopoulis, A. T. Poortinga, and M. Postema, Physics Procedia **70** 1079 (2015).
25) S. Kotopoulis, K. Johansen, O. H. Gilja, A. T. Poortinga, and M. Postema, Acta Phys. Polon. A **127** 99 (2015).
26) N. Kudo, IEEE Trans. Ultrason. Ferroelect. Freq. Control **64** 273 (2017).
27) S. Imai and N. Kudo, IEEE Int. Ultrason. Symp. **IUS2018** 184 (2018).